

## Circulation signature of vortical structures in turbulent boundary layers

Q. Gao, C. Ortiz-Dueñas and E. K. Longmire

Department of Aerospace Engineering & Mechanics  
University of Minnesota, Minneapolis, MN, 55455, USA

### Abstract

The strength of vortical structures in a turbulent boundary layer is of interest in determining the generation and development of hairpin vortices. The dual-plane Particle Image Velocimetry (PIV) data at  $z^+ = 110$  ( $z/\delta = 0.09$ ) and  $z/\delta = 0.53$  ( $z^+ = 575$ ) in a turbulent boundary layer at  $Re_\tau = 1160$  obtained by Ganapathisubramani *et al.* [7] were used to characterize the strength of the vortical structures by their circulation. The 3D-swirl was used to identify the vortex cores. The average number of swirl cores per field identified at  $z^+ = 110$  was approximately twice the average number at  $z/\delta = 0.53$ . The mean radius of the cores was found to decrease with increasing wall-normal distance. The main eigenvector of the velocity gradient tensor was used to determine the orientation of each vortex core. Circulation of the vortical structures was then calculated using the vorticity vector projected onto the main eigenvector direction. At  $z/\delta = 0.53$ , the mean circulation calculated using the eigenvector was almost the same as that using the full vorticity vector, but for  $z^+ = 110$  the mean circulation calculated using the eigenvector was 12% less than the mean circulation calculated using the vorticity vector.

### Introduction

A primary feature of turbulent boundary layers is the “hairpin vortex” originally proposed by Theodorsen [14]. Hairpin vortices can be found both in the logarithmic region and in the outer wake region and have been observed to form spatially coherent groups termed “hairpin packets” (Adrian *et al.* [2], Ganapathisubramani *et al.* [5]). These packets are an important feature as they sustain the turbulence transport and production near the wall. For instance, Ganapathisubramani *et al.* [5] found that hairpin packets can contribute more than 25% to the  $-\overline{uw}$  Reynolds shear stress while occupying less than 4% of the total area. Although the existence of these packets has been demonstrated, their generation and development is not yet well understood. Smith *et al.* [13] offered a description for the autogeneration of hairpin vortices from a single hairpin structure. They concluded that the gradient of shear forces across the boundary layer significantly affected the growth and deformation. Zhou *et al.* [15] used direct numerical simulation (DNS) to investigate the development of a single vortical structure by systematically varying its vorticity strength and wall-normal position. They found that when the vorticity strength exceeded a threshold, for a particular wall-normal distance, the vortical structure auto-generated secondary and tertiary hairpin vortices at both downstream and the side of the original hairpin vortex, which had a similar manner as that described by Smith *et al.* [13]. The primary and the new hairpin vortices subsequently developed into a coherent hairpin packet. On the other hand, they found that weaker vortical structures remained unaltered and did not auto-generate vortices. In this study, it should be noted that the single hairpin was inserted into an otherwise quiescent flow with a turbulent mean profile, and therefore, the overall flow was not fully turbulent. In a turbulent boundary layer, many vortical structures are present and thus their influence and interaction with one another could significantly affect the autogeneration pro-

cess. Nevertheless, previous studies give a useful insight into hairpin packet formation.

It is clear that the strength of the vortical structures and their wall-normal position is an important characteristic that will determine their development. Therefore, it is important to quantify the strength of vortex cores found within turbulent boundary layers. A few previous studies, e.g. Acarlar and Smith [1], Carlier and Stanislas [4], and Hambleton [9], have used circulation to characterize the strength of vortical structures. For example, Carlier and Stanislas [4], who examined planes normal to and inclined from the boundary layer surface, concluded that the circulation of vortical structures in the logarithmic region slowly decreased away from the wall mainly due to a decrease in vorticity strength and not due to a change in vortex core radius. Hambleton [9], who examined streamwise/wall-normal planes, found a similar trend for circulation. In the previous studies, only one vorticity component, that normal to the measurement plane, was available, and therefore, all vortices were assumed to have orientation normal to the measurement plane.

The aim of this study is to evaluate the strength of vortical structures crossing streamwise/spanwise planes, both in the log region and in the outer wake region. An accurate calculation of circulation requires the correct identification of the orientation of each vortex core. Thus, this study utilized data containing the full velocity gradient tensor. As will be shown, the local vorticity vector is sometimes not sufficient to determine the core direction. Other researchers ([3], [15]) noted that the local vorticity vector was not always aligned with the direction of vortical structures in simulations of channel flow. For instance, Bernard *et al.* [3] showed that the local vorticity vector was often angled away from the local axes of vortical structures at locations very close to the wall. In the current study, the eigenvector of the velocity gradient tensor was used to determine the direction of the vortical structures and eventually the circulation. In the following sections, we discuss the dataset utilized for the analysis, our methods for determining the location, size, and orientation of vortex cores, and resulting distributions of vortex orientation, size, and circulation.

### Description of PIV Dataset

The dual-plane PIV data within the log region at  $z^+ = 110$  ( $z/\delta = 0.09$ ) and within the outer wake region at  $z/\delta = 0.53$  ( $z^+ = 575$ ) of a turbulent boundary layer at  $Re = 1160$  obtained by Ganapathisubramani *et al.* [7] were investigated. The experiments were conducted in a suction-type boundary layer wind tunnel with zero pressure gradient and a freestream velocity of 5.9 m/s. The measurement plane was located 3.3 m downstream of a trip wire, and the boundary layer thickness,  $\delta$ , at the measurement plane was 70 mm. The Reynolds number based on momentum thickness  $Re_\theta$  was 2800. The coordinates  $x$ ,  $y$ ,  $z$  denote the streamwise, spanwise and wall-normal directions respectively. The results are non-dimensionalized using the skin friction velocity ( $u_\tau$ ) and the kinematic viscosity ( $\nu$ ), and are denoted with the superscript +.

A three-camera polarization-based dual plane PIV system was

used to obtain data to calculate complete velocity gradients in the lower plane. The field of view was  $1.1\delta \times 1.1\delta$ , and the resolution of each velocity vector was  $24 \times 24$  wall units. The dataset for  $z^+ = 110$  comprised of 1201 statistically-independent vector fields containing  $100 \times 100$  overlapped vectors, and the dataset for  $z/\delta = 0.53$  comprised of 912 statistically-independent vector fields containing  $95 \times 95$  overlapped vectors. Details of the experimental technique and of the mean and R.M.S. statistics of the velocity and vorticity components are given in Ganapathisubramani *et al.* [6] and Ganapathisubramani *et al.* [7].

### Vortex Identification

The swirl strength (see Zhou *et al.* [15]) was used to identify vortex cores. A technique similar to that used by Ganapathisubramani *et al.* [7] was applied. Both three-dimensional swirl,  $\lambda_{3D}^+$ , and two-dimensional swirl,  $\lambda_{2D}^+$  were employed. These are defined, respectively, as the imaginary part of the complex eigenvalue of the complete velocity gradient tensor and the imaginary part of the complex eigenvalue of the reduced velocity gradient tensor (in the x-y plane). The following steps were used in an algorithm to identify the vortex cores for each instantaneous velocity field:

- Step 1. Identified points must satisfy two conditions:  $\lambda_{3D}^+ > 0.02$  and  $\lambda_{2D}^+ > 0$ . The first condition identifies swirling regions of any orientation with dimensionless swirl strength above a threshold. This threshold, which was the same for both measurement planes, was set equal to 10% of the maximum swirl strength measured at  $z/\delta = 0.53$  (the maximum swirl strength at  $z^+ = 110$  was 0.3). The threshold value was set to minimize noise contributions to the statistics. The second condition was applied to limit identified cores to those that have some component normal to the measurement plane [12].
- Step 2. All points of local  $\lambda_{3D}^+$  maxima were marked.
- Step 3. A region growing algorithm was applied to each local maximum in order to identify core regions. If multiple vortex cores connected to each other, saddle points were located and the joint area was separated into independent vortex cores.
- Step 4. A minimum core area of 5 points was specified. The threshold for minimum number of points was used to eliminate weaker cores and potential contributions due to measurement uncertainty. Figure 1 shows results from instantaneous fields at  $z^+ = 110$  and at  $z/\delta = 0.53$ . Vortex cores identified by the algorithm are surrounded by thick black contours. It can be seen that small regions of high  $\lambda_{3D}^+$  are not identified as cores. The plots also show that the number of cores identified at  $z^+ = 110$  is larger than the number at  $z/\delta = 0.53$ . The average number of cores identified per field at  $z^+ = 110$  was approximately twice the average number at  $z/\delta = 0.53$ .

### Determining Vortex Core Orientation

In the following discussion, we will consider a vortex core as being a cross section of a swirl isosurface tube. The vortex core orientation, in particular the direction of the swirl isosurface tube, is critical to the calculation of the circulation. The orientation of vortex cores has been previously assumed to be given by the vorticity vector (e.g. Ganapathisubramani *et al.* [7]). However, as will be shown here, the direction of a swirl isosurface tube does not always match the direction given by the

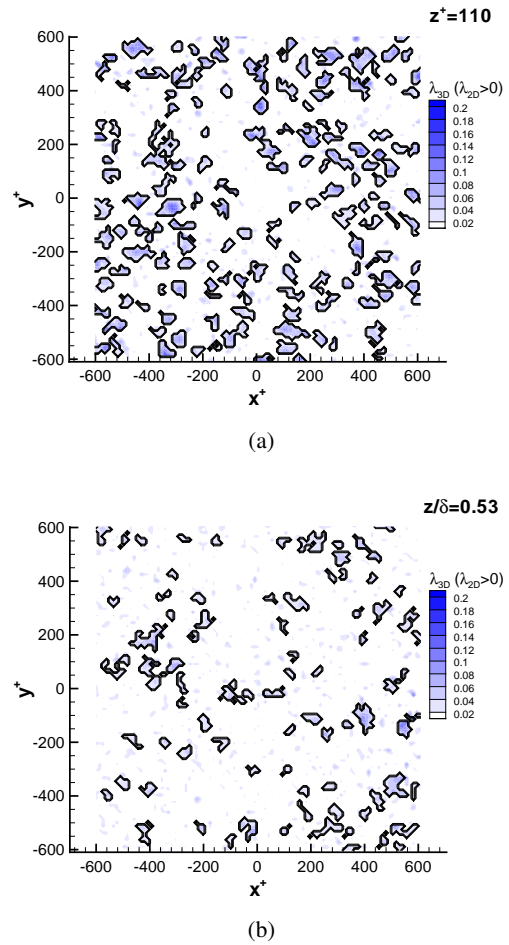


Figure 1: Identified vortex cores at (a)  $z^+ = 110$  and (b)  $z/\delta = 0.53$ . The flow is from left to right.

vorticity vector. To investigate this further, consider an incompressible flow with velocity field defined as in Equation (1) and illustrated in Figure 2:

$$\begin{bmatrix} U \\ V \\ W \end{bmatrix} = \begin{bmatrix} y-x/r \\ -x-y/r \\ z/r \end{bmatrix}, \quad r = \sqrt{x^2 + y^2}. \quad (1)$$

Figure 2(a) shows streamlines for this field while Figure 2(b) shows vortex lines. The cylindrical contour represents an isosurface of 3D-swirl for which the z axis is the axis of symmetry. The small windows in each bottom-right corner show the top views of each field. In Figure 2(b), from the top view, it is clear that the vortex lines align with the isosurface of the swirl. Since the tangent direction of the vortex lines is the direction of the vorticity vector, the direction of the vortex lines obviously differs from the direction of the z axis. Hence, for this case, the direction of the vorticity vector does not indicate the direction of the swirl isosurface tube.

Consequently, the following question arises: how can the direction of the swirl isosurface tube be determined? As mentioned previously, the 3D-swirl is defined as the imaginary part of the complex eigenvalue of the velocity gradient tensor. In a Cartesian reference frame, the velocity gradient tensor is defined as,

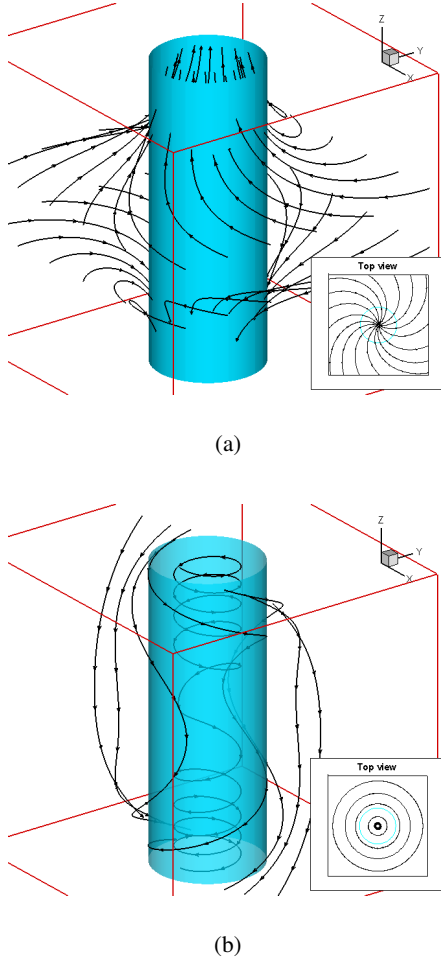


Figure 2: Illustration of flow field described by equation (1). The shaded cylinder indicates an isosurface of 3D-swirl. (a) streamlines of the velocity field; (b) vortex lines. Small windows are top view of each field.

$$\mathbf{D} = \begin{bmatrix} \frac{\partial u}{\partial x} & \frac{\partial u}{\partial y} & \frac{\partial u}{\partial z} \\ \frac{\partial v}{\partial x} & \frac{\partial v}{\partial y} & \frac{\partial v}{\partial z} \\ \frac{\partial w}{\partial x} & \frac{\partial w}{\partial y} & \frac{\partial w}{\partial z} \end{bmatrix}, \quad (2)$$

If we consider the flow in the reference frame moving with point P as illustrated in Figure 3, the velocity gradient tensor will have different matrices in different reference frames. In the case that the 3D-swirl strength is greater than zero, the tensor  $\mathbf{D}$  has one real eigenvalue,  $\lambda_r$ , and a pair of complex conjugate eigenvalues,  $\lambda_c(\cos\theta \pm i\sin\theta)$ , where  $i^2 = -1$  and  $\theta$  is the argument. In complex space, the real eigenvalue has a real eigenvector,  $\mathbf{v}_r$ , and the two conjugate complex eigenvalues have complex eigenvectors,  $\mathbf{v}_{c1}$  and  $\mathbf{v}_{c2}$ . In real space, three real eigenvectors  $\mathbf{\Lambda}_r$ ,  $\mathbf{\Lambda}_{c1}$  and  $\mathbf{\Lambda}_{c2}$  can be given by,

$$\left[ \mathbf{\Lambda}_r, \mathbf{\Lambda}_{c1}, \mathbf{\Lambda}_{c2} \right] = \left[ \mathbf{v}_r, (\mathbf{v}_{c1} + \mathbf{v}_{c2}), i(\mathbf{v}_{c1} - \mathbf{v}_{c2}) \right], \quad (3)$$

where the first unit eigenvector will be referred to as the main eigenvector.

In a non-Cartesian reference frame with these three covariant base vectors  $\mathbf{\Lambda}_r$ ,  $\mathbf{\Lambda}_{c1}$  and  $\mathbf{\Lambda}_{c2}$ , the original velocity gradient tensor,  $\mathbf{D}$ , becomes a different matrix,  $\mathbf{D}'$  defined as,

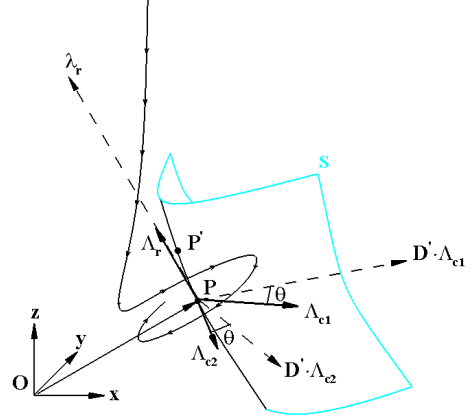


Figure 3: Streamline pattern in local covariant frame.  $\mathbf{\Lambda}_r$ ,  $\mathbf{\Lambda}_{c1}$  and  $\mathbf{\Lambda}_{c2}$  are eigenvectors of velocity gradient tensor at point P.  $\mathbf{S}$  is the swirl isosurface.

$$\mathbf{D}' = \begin{bmatrix} \lambda_r & 0 & 0 \\ 0 & \lambda_c \cos\theta & -\lambda_c \sin\theta \\ 0 & \lambda_c \sin\theta & \lambda_c \cos\theta \end{bmatrix}, \quad (4)$$

where  $\mathbf{D}'$  is the velocity gradient tensor in local non-Cartesian coordinates. Under this transition mapping, as Zhou *et al.* [15] described: every vector is either stretched or compressed by  $\lambda_r$  along the axis  $\mathbf{\Lambda}_r$ . On the plane spanned by the vectors  $\mathbf{\Lambda}_{c1}$  and  $\mathbf{\Lambda}_{c2}$ , the projection component of the vector is rotated by angle  $\theta$  and magnitude increased or decreased by  $\lambda_c$  ( $\theta$  is the angle in the  $\mathbf{\Lambda}_{c1}$ - $\mathbf{\Lambda}_{c2}$  plane, and since the base vectors are not orthogonal, this angle does not correspond with a specific rotation in the Cartesian frame.). As shown in Figure 3, the velocity variation along the  $\mathbf{\Lambda}_r$  axis is:

$$\mathbf{D}' \cdot d\mathbf{r}n_{\mathbf{\Lambda}_r} = \lambda_r d\mathbf{r}n_{\mathbf{\Lambda}_r}, \quad (5)$$

where  $d\mathbf{r}$  is a length along  $\mathbf{\Lambda}_r$  and  $\mathbf{n}_{\mathbf{\Lambda}_r} = [1, 0, 0]$  is the unit vector of  $\mathbf{\Lambda}_r$  in local non-Cartesian coordinates. In the same frame, only the  $\mathbf{\Lambda}_r$ -component of the velocity changes. The velocity gradient tensor in the  $\mathbf{\Lambda}_{c1}$ - $\mathbf{\Lambda}_{c2}$  plane will not be changed, and the strength of 3D-swirl is unchanged. The characteristic equations are the same in the different frames, and the swirl strength is an isotropic scale function of a second order tensor which depends only on the characteristic equation. Assume there is a point  $P'$  on the isosurface of swirl,  $\mathbf{S}$ , as shown in Figure 3. The vector between P and  $P'$  will limit onto  $\mathbf{\Lambda}_r$ , when  $P'$  limits toward P. Therefore,  $\mathbf{\Lambda}_r$  is the tangent to the isosurface of 3D-swirl at point P, and gives the direction of the vortex core. Thus, it has been shown that the main eigenvector gives the direction of the swirl isosurface tube.

The example presented in Figure 2 shows that, in some cases, the main eigenvector and the vorticity vector are not in the same direction. If and only if the velocity gradient tensor is the same in both Cartesian coordinates and the local covariant frame established by three real eigenvectors, the vorticity vector and the main eigenvector will be in the same direction which is the direction of the swirl isosurface tube.

## Results in Turbulent Boundary Layer

### Vortex Core Orientation

The dual plane PIV dataset of Ganapathisubramani *et al.* [7] was investigated to examine vortex cores within a turbulent boundary layer. Figure 4 gives the magnitude of the difference angle,  $\alpha$ , between the main eigenvector and the vorticity vector. The main eigenvector and the vorticity vector are the average vectors for each individual core. The positive direction of the main eigenvector  $\Lambda_r$  is defined so that the magnitude of  $\alpha$  must fall in the range (0–90°).

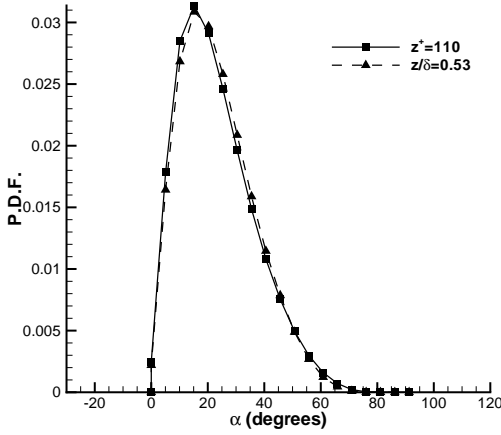


Figure 4: Probability distribution of the angle,  $\alpha$ , between the main eigenvector and the vorticity vector.

The probability distribution of the difference angle  $\alpha$  indicates a peak at approximately 15° for both wall normal positions. Note that a large number of cores appear to have a large angle difference of more than 30°. In the example flow given above, large angles occur, for example, at small  $r$  and large  $z$  magnitudes (see Figure 2(b)). In this case, the vortex lines are nearly perpendicular to the  $z$ -axis. Since Figure 4 shows only the magnitude of the angle difference, the projection angles of the vectors onto Cartesian planes are presented in Figure 5.

The projection angles of the vorticity and eigenvalue vectors in the  $y$ - $x$ ,  $y$ - $z$  and  $x$ - $z$  planes were calculated. The inclination angle  $\theta_{yx}$  is the angle made by the projection of each vector in the  $x$ - $y$  plane with the positive  $y$ -axis, such that  $\theta_{yx} = 0$  indicates alignment with the positive  $y$ -axis. The angle made by the projection of the vector in the  $y$ - $z$  plane with the positive  $y$ -axis is defined as  $\theta_{yz}$ , and  $\theta_{xz}$  is defined as the angle made by the projection of the vector in the  $x$ - $z$  plane with the positive  $x$ -axis. All of the projection angles were calculated from the average eigenvector and the vorticity vector in each individual vortex core.

Figure 5 shows the probability density function (PDF) of each of the three projection angles respectively. The closed symbols indicate angles obtained using the main eigenvector, and the open symbols indicate angles obtained using the vorticity vector. The plot of  $\theta_{yx}$  in Figure 5(a) reveals differences in the distributions at the two wall-normal locations. In the logarithmic region at  $z^+ = 110$ , both angle distributions yield peaks at  $\theta_{yx} \approx \pm 60^\circ$ , and the peaks are more distinct in the eigenvalue angle distribution. These peaks are likely caused by hairpin necks crossing the measurement plane (see [7]). The difference in the two distributions therefore suggests that the necks are better

identified by the eigenvalue angle. In the wake region at  $z/\delta = 0.53$ , the peaks at  $\pm 60^\circ$  are much weaker, if present at all, and the distributions are broader. Little difference is seen between the eigenvector and vorticity angle distributions. The larger percentage of structures with  $\theta_{yx}$  near  $0^\circ$  suggests that more hairpin heads are crossing this plane. The distinct increase in the percentage of cores with orientation around  $\pm 180^\circ$  suggests the presence of cores with rotation opposite to hairpin heads as observed previously by Adrian *et al.* [2] and Carlier and Stanislas [4].

Figure 5(b) corresponding with  $\theta_{yz}$  reveals similar distributions at the two wall normal locations. At both locations, the eigenvector distribution yields a sharper peak than the vorticity distribution, and the peaks are shifted toward larger angles. If the distributions are interpreted in terms of hairpin vortices, the peaks correspond with tilt angles of hairpin necks in the spanwise direction. Thus, the increase in the peak angle suggests that the neck cores are tilted more to the vertical than previously thought (see [7]).

The inclination angle  $\theta_{xz}$  is the angle discussed most frequently in descriptions of boundary layer structure. The angle distributions, plotted in Figure 5(c), show a clear difference between those calculated using the main eigenvector and the vorticity vector. The projection angle obtained using the main eigenvector peaks at  $\theta_{xz} = 50^\circ$  and  $-130^\circ$  at  $z^+ = 110$  and  $\theta_{xz} = 60^\circ$  and  $-120^\circ$  at  $z/\delta = 0.53$ . This is consistent with previous results of other researchers where  $\theta_{xz}$  was seen to increase with wall normal position ([3], [8], [10], [11]). On the contrary, the results based on the vorticity vector suggest that the most probable  $\theta_{xz}$  decreases slightly with increasing wall normal position. Thus, the eigenvector identification method appears more consistent with the prevailing literature.

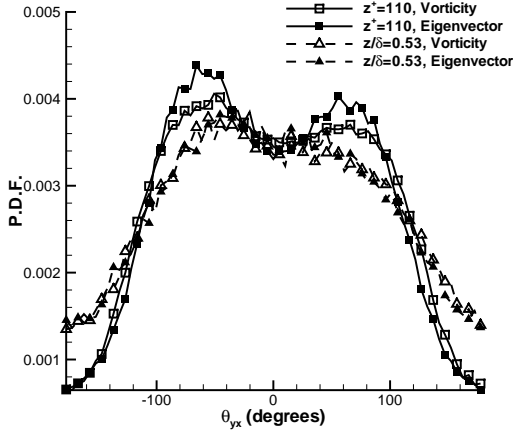
### Circulation

To investigate the generation and development of hairpin vortices in turbulent boundary layers, one important issue is identifying the strength of the vortical structures. The traditional concept of circulation is introduced. The circulation was calculated for each vortex core using equation 6,

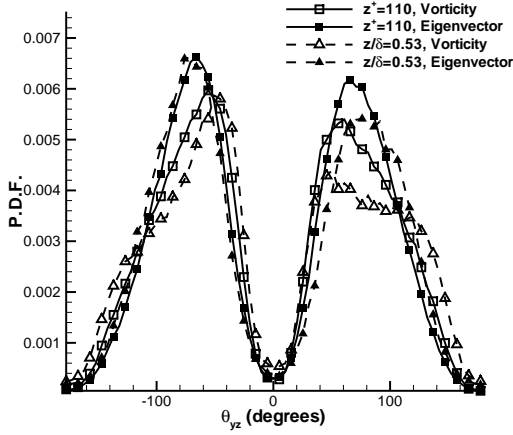
$$\Gamma^+ = \int_A (\omega^+ \cdot \Lambda_r) (\Lambda_r \cdot \mathbf{n}_z) dA^+, \quad (6)$$

where  $A$  is the vortex core area in the  $x$ - $y$  plane (measurement plane),  $\omega$  is the vorticity vector,  $\mathbf{n}_z$  is a unit vector in the  $z$  direction, and  $\Lambda_r$  is the main eigenvector described in the previous section.

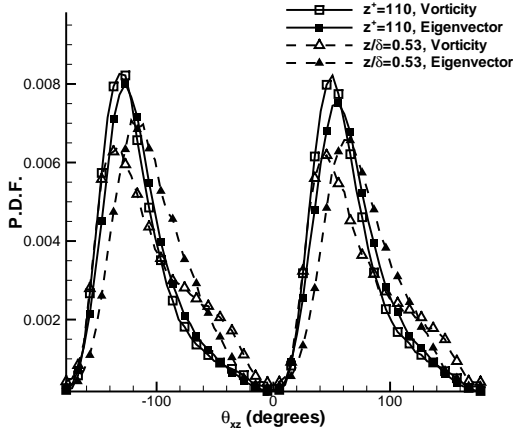
The value of circulation is affected by the size of the vortical structures and the strength of rotation about the axis of the swirl isosurface. For the PIV dataset, the vortex core area and equivalent radius were determined in two ways. First, the area was determined in the measurement plane, as was done by previous researchers ([4], [9]). Figure 6 shows the PDF of the radius of the circle with area equivalent to the vortex core area in the measurement plane for the two wall-normal positions. In this case, the mean radius  $r^+$ , was calculated to be 21.1 for  $z^+ = 110$  and 19.95 for  $z/\delta = 0.53$ . These values are of similar magnitude to the values obtained by Carlier and Stanislas [4] in other planes. They found that the mean radius  $r^+$  across the log layer of a turbulent boundary layer at  $Re_\theta = 7500$  ( $Re_\tau$  is about 2000) varies between 18 and 26. However, they concluded that the mean radius slightly increases away from the wall. This trend was not observed here, although we are examining a different plane and also comparing a position in the log layer to a position in the outer wake region. Figure 6 also suggests that the cores identi-



(a)



(b)



(c)

Figure 5: Probability density function of (a)  $\theta_{yx}$ ; (b)  $\theta_{yz}$ ; (c)  $\theta_{xz}$ .

fied at  $z^+ = 110$  have larger radii than the cores at  $z/\delta = 0.53$  for  $r^+$  larger than the mean.

Because of our access to the orientation of each core, we could also determine a 'true' core area and radius for each structure. The exact equivalent radius of each vortical structure,  $r'^+$ , was

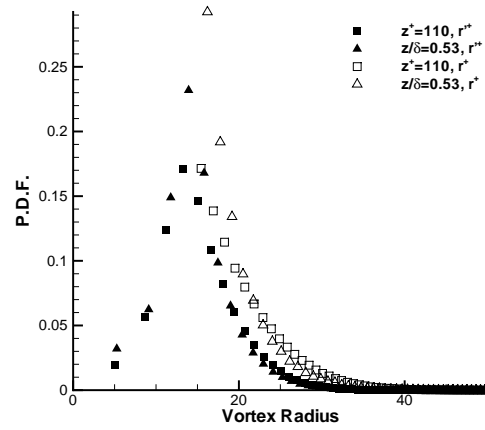


Figure 6: Probability density function of vortex core radius  $r^+$  and  $r'^+$ . Minimum area threshold to be accepted as a core has approximately a radius of 15 (equivalent to 5 contiguous points).

calculated as

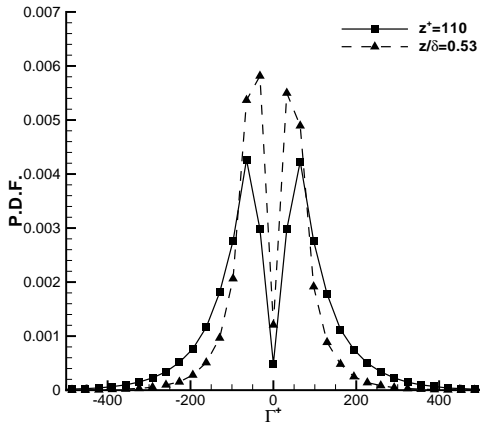
$$r'^+ = \sqrt{\bar{\Lambda}_r \cdot n_z \int_A dA^+ / \pi}, \quad (7)$$

where  $\bar{\Lambda}_r$  is the average unit eigenvector of an individual vortex core. Obviously, this radius will be smaller than  $r^+$  for all cores that are not perpendicular to the measurement plane. The mean value of  $r'^+$  was calculated as 15.1 for  $z^+ = 110$  and 14.6 for  $z/\delta = 0.53$  (see also the distributions in Figure 6). Note that the 5-point area threshold in the measurement plane was applied to these cores, and since  $r'^+$  was generally smaller than  $r^+$ , some  $r'^+$  values occur at radii less than 15 as shown in Figure 6.

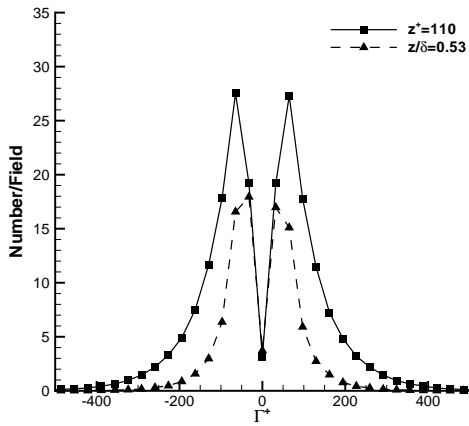
Figure 7(a) shows a comparison of the probability density function of the normalized circulation,  $\Gamma^+$ , using vorticity projected onto the main eigenvector, at  $z^+ = 110$  and  $z/\delta = 0.53$ . The dip at  $\Gamma^+ = 0$  is a result of the core selection criteria which filter out either smaller or in-plane oriented vortices. The PDF yields peaks at  $\pm 66$  for  $z^+ = 110$  and at  $\pm 33$  for  $z/\delta = 0.53$ . Furthermore, the mean of the magnitude of the circulation,  $\Gamma^+$ , was calculated to be 106.4 for  $z^+ = 110$  and 68.8 for  $z/\delta = 0.53$ . These results suggest that the mean strength of the vortical structures decreases with wall-normal distance. When the mean circulation per core was calculated using vorticity parallel to the vorticity vector, the magnitude was approximately the same at  $z/\delta = 0.53$ , but for  $z^+ = 110$  the mean circulation calculated using the eigenvector was 12% smaller than the mean circulation calculated using the vorticity vector. This suggests that the correct identification of the vortex core normal direction becomes more critical in regions closer to the wall.

Figure 7(b) shows the number distribution of cores identified per field for the two wall-normal distances. The weaker, narrower curve obtained for  $z/\delta = 0.53$  illustrates the smaller number of cores identified for this wall-normal position, of approximately half, as mentioned earlier. In addition, the distribution shows that there are larger numbers of cores at  $z^+ = 110$  for all circulation values in the range  $50 < \Gamma^+ < 300$ .

These results show that, in the log region ( $z^+ = 110$ ), the vortex cores are both more numerous and stronger than in the outer wake region ( $z/\delta = 0.53$ ), as shown by the higher values of



(a)



(b)

Figure 7: (a) Probability density function of circulation  $\Gamma^+$ . (b) Absolute number of cores identified per field.

circulation  $\Gamma^+$ , and the large number of cores with higher circulation. Stronger and more numerous vortices within the log region possibly indicates that the autogeneration of new hairpin vortices is more likely to occur at this wall normal location and therefore more hairpin packets are likely to form. This hypothesis is consistent with the findings of Zhou *et al.* [15] who postulated that, as  $z^+$  increased above 50, increasingly strong vortices would be required for autogeneration of packets in their simulated flow. It is also consistent with the experimental findings of Ganapathisubramani *et al.* [5] who concluded that, within the log region, streamwise spatial coherence and organization characteristic of hairpin packets were observed whereas in the outer wake region, only single vortex cores were identified.

In order to compare the present results with the earlier numerical investigation of Zhou *et al.* [15], they are replotted in Figure 8 in terms of the average vorticity magnitude within each core (here, unlike the circulation distributions, the vorticity magnitude is determined from the full vorticity vector). The distributions can be compared with the vorticity threshold for autogeneration of packets proposed by Zhou *et al.* [15]. In that study, the authors proposed that vortical structures exceeding a threshold vorticity strength can generate secondary and tertiary vortices. These new hairpin vortices can subsequently develop into coherent packets. In order to compare the present results

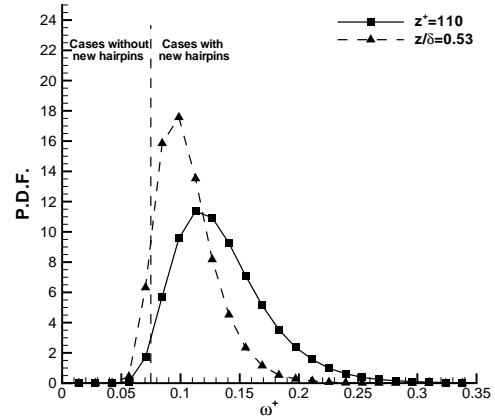


Figure 8: Probability density function of average vorticity magnitude  $\omega^+$  in each core. The dashed line indicates the vorticity strength threshold proposed by Zhou *et al.* [15] for  $z^+ = 110$  necessary for autogeneration of secondary and tertiary vortices.

with the threshold found by Zhou *et al.* [15], their threshold values were re-normalized using inner scale variables, i.e., the skin friction velocity  $u_\tau$  and the length scale  $l = \nu/u_\tau$ . Zhou *et al.* [15] estimated a threshold of approximately  $\omega^+ = 0.075$  equivalent to  $\alpha = 2.6$  in their notation, for a wall normal position of  $z^+ = 110$  beyond which a primary vortex can autogenerate secondary and tertiary vortices. (No threshold for larger  $z^+$  was available in their results).

The PDF in Figure 8 yields peaks at  $\omega^+ = 0.12$  for  $z^+ = 110$  and at  $\omega^+ = 0.084$  for  $z/\delta = 0.53$ . This indicates that the average vortex strength, in terms of vorticity, decreases with increasing wall-normal distance. Comparing the PDF of vorticity magnitude with the threshold proposed by Zhou *et al.* [15] indicates that 97% of the cores identified at  $z^+ = 110$  can autogenerate new vortices. This comparison is misleading for multiple reasons, however. First, the DNS of Zhou *et al.* [15] is not a fully turbulent flow. As described earlier, the DNS contains a mean velocity profile corresponding with a turbulent channel flow, but only one eddy event is imposed on the mean. Therefore, the simulation ignored the effects of the numerous interacting eddies in real turbulent flow. In a real boundary layer, the event threshold required for initiation of a hairpin packet may be significantly higher than in the simulated flow. Second, although we have compared average vorticity values, we have not incorporated vortex core area in our comparison. It is likely that the events leading to autogeneration in the simulated flow led to vortex core radii that were large on average compared with the full distribution of core sizes. Therefore, it would be better to compare circulation directly (which we plan to do in the near future).

Although no threshold data are available from the study by Zhou *et al.* [15] for the outer-wake region, the threshold is expected to be higher in that region, and thus the percentage of vortex cores with the likelihood of generating new hairpin vortices is expected to decrease significantly. For example, given the data in Figure 8, if the threshold were to be doubled from the one presented, only 4% of the cores identified at  $z/\delta = 0.53$  could be considered to potentially autogenerate new vortices.

The results shown here are an initial step into understanding the evolution of vortical structures within the boundary layer. In reality, the development of a hairpin vortex will occur in the

presence of other vortices which could influence and interact with the hairpin vortex thus affecting the autogeneration process. Merging of vortices to form larger structures could also occur. Nevertheless, the results here provide an initial step into understanding the nature of the vortex structures in the boundary layer.

## Conclusions and Discussion

The orientation and circulation of vortical structures within the log region and the outer wake region in a turbulent boundary layer have been investigated. Based on this investigation, the following conclusions were obtained:

- The average number of swirl cores identified per field in the log region was approximately twice the average number identified in the outer wake region.
- The orientation of the vortex cores, identified using 3D-swirl, is best given by the eigenvector of the velocity gradient tensor and not the vorticity vector.
- The mean radii of the vortex cores corresponding with swirl isosurface tubes was found to decrease with increasing wall-normal distance.
- In the log region ( $z^+ = 110$ ), vortex cores had a higher mean circulation than the cores in the outer wake region ( $z/\delta = 0.53$ ).
- Using the eigenvector instead of the vorticity vector to determine the direction of vortical structure resulted in a decrease of the mean circulation per core of 12% at  $z^+ = 110$  and almost no decrease at  $z/\delta = 0.53$ . This suggests that the correct identification of the vortex core orientation is an important issue, and it becomes more critical in regions closer to the wall.

The results we provided here represent an initial step into understanding the nature of the vortex structures in the turbulent boundary layer. In the near future, more aspects will be investigated such as:

- The effect of Reynolds number on vortex core size and the circulation. Head and Bandyopadhyay [10] pointed out that the radii of hairpin cores are likely to decrease with increasing Reynolds number. It will be very interesting to understand the relations between Reynolds number and the radii of hairpin cores qualitatively and quantitatively. At the same time, in order to isolate this scaling dependence from other effects, it would again be important to determine the effect of Reynolds number on circulation statistics.
- The distribution of vortex cores in different orientation planes and different wall normal locations. Previous research examining vortex cores provided results in different orientation planes. Carlier and Stanislas [4] focused on the spanwise-wall normal plane and its tilt planes. Hambleton [9] mainly took measurements in streamwise-wall normal planes. Both of them provided the trend of vortex cores changing with the wall normal direction. Currently, we have datasets in only two wall normal locations. It will be interesting to have more data in different locations to compare against the previous investigations.
- The development and dynamics of vortical structures in turbulent boundary layers. Since the strength of the vortical structures was qualified successfully as we showed,

it will be valuable to apply the techniques herein in time-evolving flow fields.

## Acknowledgements

Financial support from the National Science Foundation through Grant No. CTS-0324898 is gratefully acknowledged.

## References

- [1] Acarlar, M.S. and Smith, C.R., A study of hairpin vortices in a laminar boundary layer, Part 1: hairpin vortices generated by a hemisphere protuberance, *J. Fluid Mech.*, **175**, 1987, 1-41.
- [2] Adrian, R.J., Meinhart, C.D. and Tomkins, C.D., Vortex organization in the outer region of the turbulent boundary layer., *J. Fluid Mech.*, **422**, 2000, 1-54.
- [3] Bernard, P.S., Thomas, J.M. and Handler, R.A., Vortex dynamics and the production of Reynolds stress, *J. Fluid Mech.*, **253**, 1993, 385-419.
- [4] Carlier, J. and Stanislas, M., Experimental Study of eddy structures in a turbulent boundary layer using particle image velocimetry, *J. Fluid Mech.*, **535**, 2005, 143-188.
- [5] Ganapathisubramani, B., Longmire, E.K. and Marusic, I., Characteristics of vortex packets in turbulent boundary layers, *J. Fluid Mech.*, **478**, 2003, 35-46.
- [6] Ganapathisubramani, B., Longmire, E.K., Marusic, I. and Pothos, S., Dual-plane PIV technique to measure complete velocity gradient tensor in a turbulent boundary layer, *Exp. Fluids*, **39**, 2005, 222-231.
- [7] Ganapathisubramani, B., Longmire, E.K. and Marusic, I., Experimental Investigation of vortex properties in a turbulent boundary layer, *Physics of Fluids*, **18**, 2006, 055105.
- [8] Haidari, A.H. and Smith, C.R., The generation and regeneration of single hairpin vortices, *J. Fluid Mech.*, **277**, 1994, 135-162.
- [9] Hambleton, W.T., Experimental study of coherent events in laminar and turbulent boundary layers, PhD thesis, University of Minnesota, 2007.
- [10] Head, M.R. and Bandyopadhyay, P., New aspects of turbulent boundary layer structure, *J. Fluid Mech.*, **107**, 1981, 297-338.
- [11] Marusic, I., On the role of large-scale structures in wall turbulence, *Physics of Fluids*, **13**, 2001, 735-743.
- [12] Marusic, I., Ganapathisubramani, B. and Longmire, E.K., Dual-plane PIV investigation of structural features in a turbulent boundary layer, in *Proc. 15th Australasian Fluid Mechanics Conf.*, The University of Sydney, Sydney, Australia, 13-17 Dec., 2004.
- [13] Smith, C.R., Walker, J.D.A., Haidari, A.H. and Sobrun, U., On the dynamics of near-wall turbulence, *Phil. Trans. R. Soc. Lond.*, **A 336**, 1991, 131-175.
- [14] Theodorsen, T., Mechanism of turbulence, in *Proc. Second Midwest Conf. of Fluid Mechanics*, Ohio State University, Columbus, Ohio, 1952, 1-19.
- [15] Zhou, J., Adrian, R.J., Balachandar, S. and Kendall, T. M., Mechanisms for generating coherent packets of hairpin vortices in channel flow, *J. Fluid Mech.*, **387**, 1999, 353-396.